Measurement of Near-Threshold J/ψ Quasi-real Photoproduction on the Proton and Neutron

Richard Tyson

May 2024

Abstract

This release note summarizes the steps taken towards the extraction of the total cross section of the quasi-real photoproduction of J/ψ near its 8.2 GeV production threshold on both proton and neutron targets. The data used for this analysis were taken in 2019 and 2020, with a 10.6 and 10.2 GeV electron beam scattering on a liquid deuteron target. This release note will be kept short and concise as its purpose is simply the release of the cross section in arbitrary unit.

List of figures intended for release:

- Figure 1: e^+e^- invariant mass spectra produced on the proton and neutron in all available RG-B data.
- Figure 3: Comparison of the integrated cross-section in arbitrary units produced on the proton and neutron as a function of quasi-real photon energy.

1 Introduction

It has been predicted that J/ψ photoproduction in the near-threshold region can enable access to the gluonic Gravitational Form Factors (gGFFs) [1, 2] which encode properties of the nucleon such as its mass and pressure distributions [3]. The gGFFs are defined from the matrix elements of the energy-momentum tensor (EMT) that couples to a spin-2 particle such as the graviton, the assumed force carrier of gravity [3, 4]. Accessing the gGFFs from J/ψ photoproduction relies on a two-gluon exchange that forms a spin-2 coupling between J/ψ and the nucleon [5, 6]. Two-gluon exchange VMD based models were shown to adequately describe the near-threshold J/ψ photoproduction total and differential cross sections [5, 6]. Holographic QCD can also be used to model J/ψ photoproduction based on a tensor graviton like exchange (2++) [1, 7, 8]. In the Generalised Parton Distribution (GPD) framework, large skewness at threshold allows to relate the scattering amplitude to gluon GPDs. The GFFs are extracted from the first moments of the GPDs [1, 9, 10, 11].

However, there are suggestions that near-threshold J/ψ photoproduction could be dominated by the open charm production of $\Lambda^c\overline{D}^{(*)}$ [12, 13]. This scenario would complicate the extraction of the gGFFs as there would no longer be a dominant spin-2 coupling between J/ψ and the nucleon. At present, the world data on near-threshold J/ψ photoproduction does not have the statistical precision to distinguish between the various proposed production mechanisms and additional data is required [13].

All the previous measurements of near-threshold J/ψ photoproduction have been made on the free proton using stationary liquid hydrogen targets [14, 15, 16]. This release note will present preliminary results of the first measurement of the near-threshold cross section on the bound neutron and bound proton in a liquid deuteron target. Measuring J/ψ photoproduction on both proton and neutron will bring new constraints on open-charm contributions to the cross section. Comparing the cross section on proton and neutron also allows to test the isospin invariance of the production mechanism, with a two-gluon exchange expected to be isospin invariant but not necessarily open-charm production of J/ψ p. Finally, additional data of near-threshold J/ψ photoproduction, whether on the free or bound proton, will be required to distinguish between the proposed J/ψ production mechanisms.

2 Datasets

Three datasets are used for this measurement, all taken within the Run Group B (RG-B) experiment. The *spring2019* data was taken in the spring of 2019 with a 5cm liquid deuteron (LD_2) target. The *fall2019* and *spring2020* data were taken with the same target in the fall of 2019 and spring of 2020. The *spring2019* and *spring2020* datasets used inbending torus polarity, with the *fall2019* using outbending. All three datasets were cooked with so called pass2 reconstruction. The *spring2019* dataset was taken at two different beam energies. Roughly 40% of data was taken at 10.5986 GeV, with roughly half taken with a 35 nA beam current and the other half taken at 50 nA. The other 60% of the *spring2019* dataset was taken at 10.1998 GeV with a 50 nA beam current. The accumulated charge at 10.5986 GeV is of 27.01 mC, with the accumulated charge at 10.1998 GeV being 39.39 mC. The *fall2019* dataset was taken at 10.410 GeV with 40 nA beam current, accumulating 12.85 mC. The *spring2020* dataset was taken at 10.389 GeV with a 50 nA beam current, accumulating 28.4 mC. The analysis uses the QADB golden run definition established using the pass 1 reconstruction, this will be updated once the pass 2 version of the QADB is available.

The simulated data is produced with *GEMC*[17]. Events are generated with *elSpectro*[18], an all purpose event generator which allows to correctly generate photo and electro production of mesons and baryons at experiments such as CLAS12 or others. *elSpectro* will simulate the Fermi motion of the bound constituents of the nucleon and can either be set up to use the JPAC predictions for the J/ψ photoproduction cross section, or without placing constraints on the kinematics of the J/ψ decay. The later option was used here. The simulations are produced at different beam energies and with background merging corresponding to different beam currents, with the same proportion of each as to that in the three datasets. Background merging is not yet available for the *spring2020* dataset and so the background merging and configuration (gcard) for the 10.2 GeV 50nA *spring2019* data was used instead.

3 Analysis Procedure

For the analysis of J/ψ photoproduction, all final state particles are detected in the CLAS12 Forward Detector (FD) [19]. The High Threshold Cherenkov Counter (HTCC) was built to identify electrons [20]. The Drift Chambers (DC) measure the charge and momentum of charged particles [22]. The Forward Time Of Flight (FTOF) counters were designed to identify charged hadrons [23]. The Electromagnetic Calorimeters (PCAL and EC) are used to detect neutrals [24].

In the RG-B experiment, an electron beam is incident on the stationary deuteron target. The reactions $ep_{bound} \rightarrow e'J/\psi p \rightarrow (e')e^+e^-p$ and $en_{bound} \rightarrow e'J/\psi n \rightarrow (e')e^+e^-n$ are being measured in untagged quasi-real photoproduction, where all the final state particles (the nucleon(s) and the lepton pair from the J/ψ decay) are detected in the FD. The *bound* subscript for the target nucleons refers to the fact that these are the constituent protons and neutrons in the deuteron target. Since the aim is to extract the J/ψ photoproduction cross section, we are interested in events where the four-momentum transfer, Q^2, to the virtual photon is close to zero, i.e. where the photon is quasi-real. The interacting beam photon and the undetected scattered electron kinematics are deduced from 4-momentum conservation. The J/ψ meson is reconstructed by means of its di-lepton decay, either e^+e^- or $\mu^+\mu^-$. Here only the analysis in the e^+e^- is shown although consistency in the measured cross section with the $\mu^+\mu^-$ decay channel has been shown for pass 1 reconstruction [25].

The first step of the analysis of J/ψ photoproduction is to identify the final state particles. Electrons and positrons are required to produce a signal in the HTCC and have a ratio of their energy deposition to momentum around 0.25. Muons are minimum ionising particles which are selected with cuts on their energy deposition in the calorimeters. Muons are required to have a low energy deposition whilst electrons are required to have a high energy deposition. This allows to unambiguously separate muons and electrons. The event builder identification (two photoelectrons in the HTCC and sampling fraction cut) is required for electrons and positrons. Positron identification is then refined by training a boosted decision tree classifier [26] on variables from several CLAS12 detector subsystems, such as energy deposition, cluster information in the calorimeters, and the number of photoelectrons produced in the HTCC. Ref. [25] demonstrates in detail how a cleaner positron (and muon) identification can be achieved by using such machine learning classifiers. To identify protons the time-of-flight technique is used by means of a cut on the event distribution of speed versus momentum. Only the event builder identification is used for the proton. A neutral charge only is required to identify neutrons. No further identification procedures were applied for neutrons as there is not any strong evidence of photon contamination.

Electrons and positrons may radiate photons before they are detected in the FD. The momentum of photons with a small polar angle difference to electrons and positrons is added back to the electrons and positrons to correct their reconstructed momentum. The path length determination of neutrons is known to be complicated due to the thickness of the calorimeter and the unknown interaction point inside the calorimeter. The default average distance is taken as the front face of the calorimeters. Momentum dependent corrections are established using exclusive reactions such as $ep \rightarrow e'\pi^+ n$ and comparing the reconstructed momentum to the missing momentum calculated without the neutron. Finally, a single neutron track can lead to multiple reconstructed neutrons in the FD. This effect is seen in both simulation and real data. This effect can be due to real physical processes where a neutron interacting with the calorimeter produces secondary particles which are then reconstructed as neutrals. This effect can also be due to issues in the clustering which creates multiple clusters for a single neutron. The initial neutron (first in time) is selected to avoid having multiple neutron candidates in a given event.

Once the final state particles are identified, events consistent with the quasi-real photoproduction of a di-lepton pair are selected by removing high Q^2 events. The invariant mass of missing particles in the reaction $eN_{bound} \rightarrow (e')l^+l^-N$ is required to be consistent with that of the undetected scattered electron. The e^+e^- invariant mass is then fitted in bins of the energy E_γ of the incident photon to determine the total cross section as a function of E_γ. The J/ψ peak is fitted with a gaussian, whilst several background functions were investigated, including a second or third order polynomial and an exponential function. These give consistent estimates of the cross section. Figure 1 shows the e^+e^- invariant mass close to the J/ψ mass for e^+e^- produced on the proton and neutron and combining all datasets. More detail on the analysis procedures described above can be found in Ref. [25].

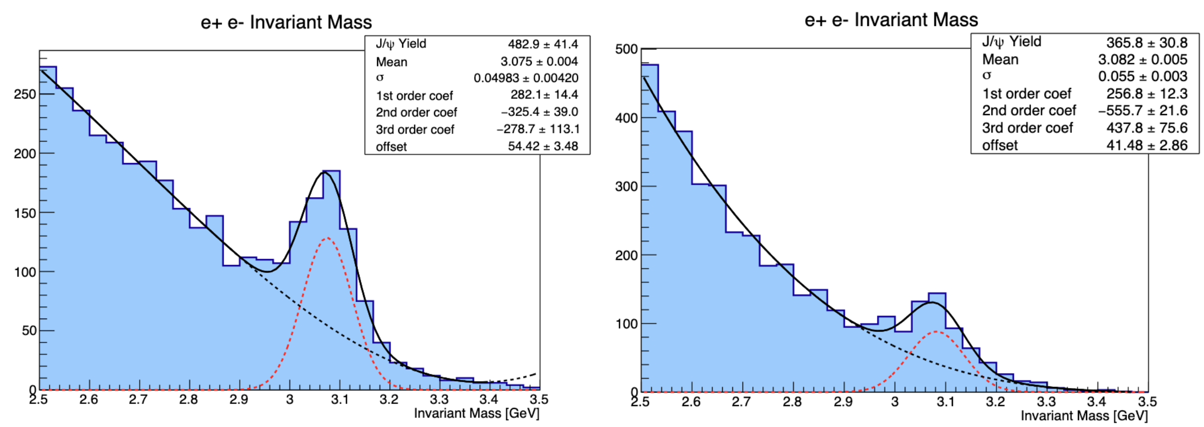

Figure 1: The e^+e^- invariant mass produced on proton (left) and neutron (right) combining all three datasets.

4 Cross Section

The total cross section $\sigma_0(E_\gamma)$ is measured as a function of quasi-real photon energy and is calculated using Equation 1 below.

$$\sigma_0(E_\gamma) = \frac{N_{J/\psi}(E_\gamma)}{N_\gamma \cdot \rho_T \cdot l_T \cdot \omega_c \cdot Br \cdot R_c \cdot \epsilon(E_\gamma)} \tag{1}$$

$N_{J/\psi}$ refers to the number of J/ψ measured in each bin of quasi-real photon energy. This is measured as shown in Figure 1 by fitting the di-lepton invariant mass. The acceptance ϵ measured in bins of E_γ accounts for the FD detection and reconstruction efficiency, its geometrical acceptance and the impact of analysis procedures on $N_{J/\psi}$. This is measured in simulation by taking the ratio of the number of generated (true/thrown) events to that of the reconstructed events in bins of E_γ.

The product $N_\gamma \cdot \rho_T \cdot l_T \cdot Br$ in the denominator of Equation 1 normalises the number of J/ψ produced based on the experiment and reaction to give the cross section. l_T is the target length (5cm), with ρ_T the number of protons or neutrons in the target, calculated as:

$$\rho_T = N_N = 2N_{molecules} = 2N_A \frac{\rho}{M} \tag{2}$$

for ρ_T the target density equals to the number of nucleons N_N, which is twice the number of molecules $N_{molecules}$ of LD_2, N_A Avogadro's number, ρ the physical density and M the molar mass. For deuteron, the physical density is $\rho = 0.163$ g cm^{-3} with the molar mass $M = 4.028$ g mol^{-1}. The number of protons or neutrons in the LD_2 target is therefore $\rho_T = 4.87 \cdot 10^{22}$ nucleons per cm^{-3}. The length l_T of the LD_2 target is $l_T = 5$ cm. N_γ refers to the number of real and virtual photons per GeV calculated as:

$$N_\gamma = \frac{Q(F_R + F_V)}{q} \tag{3}$$

where Q is the accumulated charge of the dataset, q is the electron charge $q = 1.6 \cdot 10^{-19}C$ and F_R and F_V the real and virtual photon flux respectively. The real photon flux is due to real bremsstrahlung photons produced inside the target and target cell as the electrons from the beam interact with the electric field of the constituent protons and neutrons of the target or target cell. The real photon flux per GeV is calculated as:

$$F_R = \frac{1}{E_\gamma}\left(\frac{l_T}{2X_{0\_}T} + \frac{l_c}{X_{0\_}c}\right)\left(\frac{4}{3} - \frac{4}{3} \times \frac{E_\gamma}{E_b} + \frac{E_\gamma^2}{E_b^2}\right) \tag{4}$$

for X_0 and l the scattering length and length of the target (T) and target cell (c) and E_b the electron beam energy. The factor of a half for the target contribution comes from the fact that bremsstrahlung photons are produced throughout the target, with a photon produced at the end of the cell having a lower probability of interacting with the target and therefore a lower contribution to the luminosity. This effect works out to a factor of a half on average.

The virtual photon flux is due to the virtual photons mediating the interaction of the electron beam with the target. This can be calculated based on the equivalent photon approximation (EPA) as:

$$F_V = \frac{1}{E_b} \times \frac{\alpha}{x\pi}\left((1 - x + \frac{x^2}{2})log\left(\frac{Q^2_{max}}{Q^2_{min}}\right) - (1-x)\right) \tag{5}$$

where $x = \frac{E_\gamma}{E_b}$, $Q^2_{min} = M_e^2 \frac{x^2}{(1-x)}$ and Q^2_{max} a free parameter, for M_e the mass of an electron and α the fine structure constant. A comparison of the real and virtual photon flux for the RG-B LD_2 target and a 10.6 GeV beam is shown in Figure 2 below:

Br in Equation 1 is the branching ratio, which is roughly 6% for the J/ψ decay to a di-lepton pair. The product of N_γ, l_T and ρ_T describe the quasi-real photoproduction luminosity of the experiment. The branching ratio then accounts for the fact that only 6% of J/ψ will decay to an electron positron pair or a di-muon pair.

The final terms of Equations 1 are an overall normalisation factor ω_c and radiative corrections R_c. The normalisation ω_c corrects for errors in the flux or acceptance calculations. The radiative correction R_c accounts for the shift in reconstructed kinematics that occurs when one of the lepton loses energy due to radiative effect. This correction is computed in simulation as the ratio of events generated in a given bin with radiative effect and without radiative effect. Both ω_c and R_c have **not** been estimated for this release note.

The preliminary estimates of the cross section of J/ψ quasi-real photoproduction on proton and neutron in Figure 3. This is shown in arbitrary units as the overall scale of the cross sections is not known as the normalisation and radiative corrections have not yet been established. Only the statistical uncertainty on the cross section estimates is reported in Figure 3. The good agreement within the statistical uncertainty of the total cross sections produced on the proton and neutron suggests that whatever production mechanism is at play must be isospin invariant, or if isospin invariance is broken, the effect is smaller than the reported statistical uncertainty.

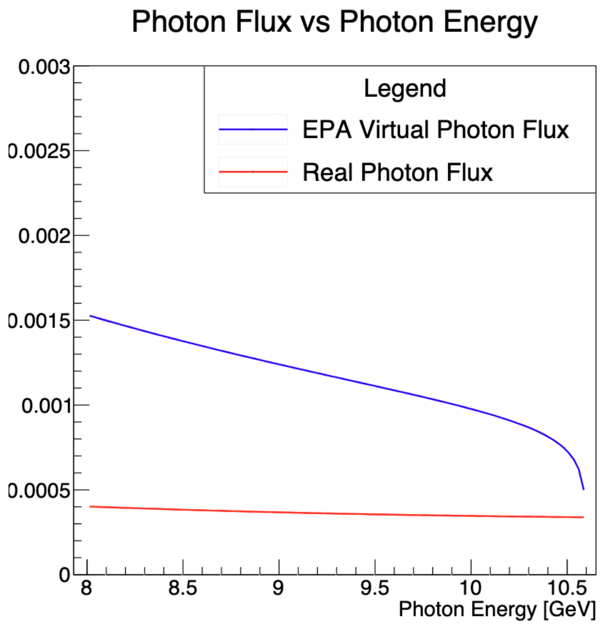

Figure 2: The real and virtual photon flux for the RG-B LD_2 target and a 10.6 GeV beam.

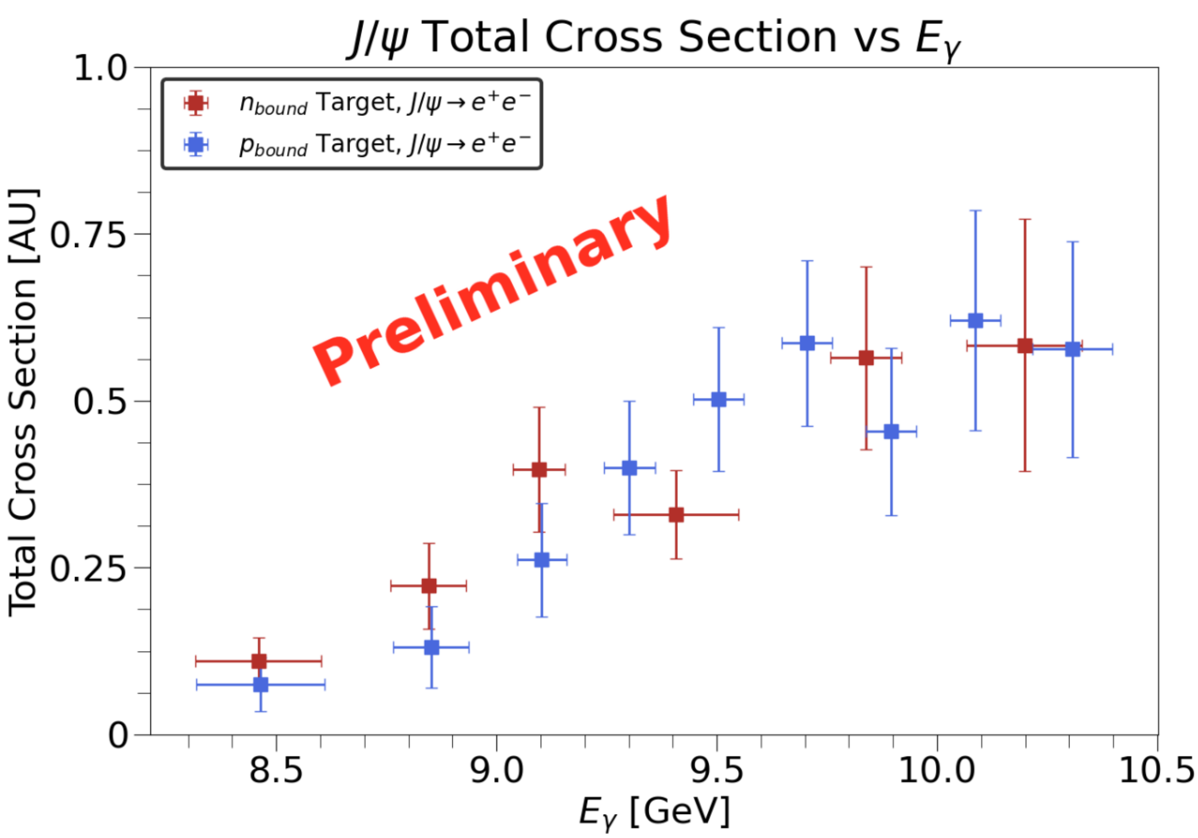

Figure 3: The near-threshold J/ψ quasi-real photoproduction cross section as a function of E_γ produced on proton (blue) and neutron (red). The cross section is shown in arbitrary units as the overall normalisation has not yet been established.

5 Consistency with Previous Measurements

N.B.: This section is not to be released.

The J/ψ photoproduction total cross section on the proton has previously been measured at GlueX [14, 15] and a CLAS12 release note recently asked for the release of the RG-A analysis of the total cross on the proton. In order to show consistency with previous measurements, the normalisation and radiative corrections from the RG-A analysis are applied to the RG-B analysis. Although not fully rigorous, it is expected that the normalisation should be similar for RG-A and RG-B. The same flux calculations are used and the data. Both experiments ran close together in time, and were reconstructed similarly, which suggests that the acceptance in both expriments is similarly mis-represented by the simulation. The radiative corrections should be the same as the proton, neutron or deuteron form factors are not used in the formulae. Figure 4 shows a comparison between the GlueX estimates of the total cross section, that from RG-A and those shown in Figure 3 but applying the normalisation and radiative corrections of the RG-A analysis. This figure is not intended for release, and is only shown here to demonstrate the good agreement between the different estimates of the cross section. In turn, this validates the consistency between the RG-A and RG-B analyses.

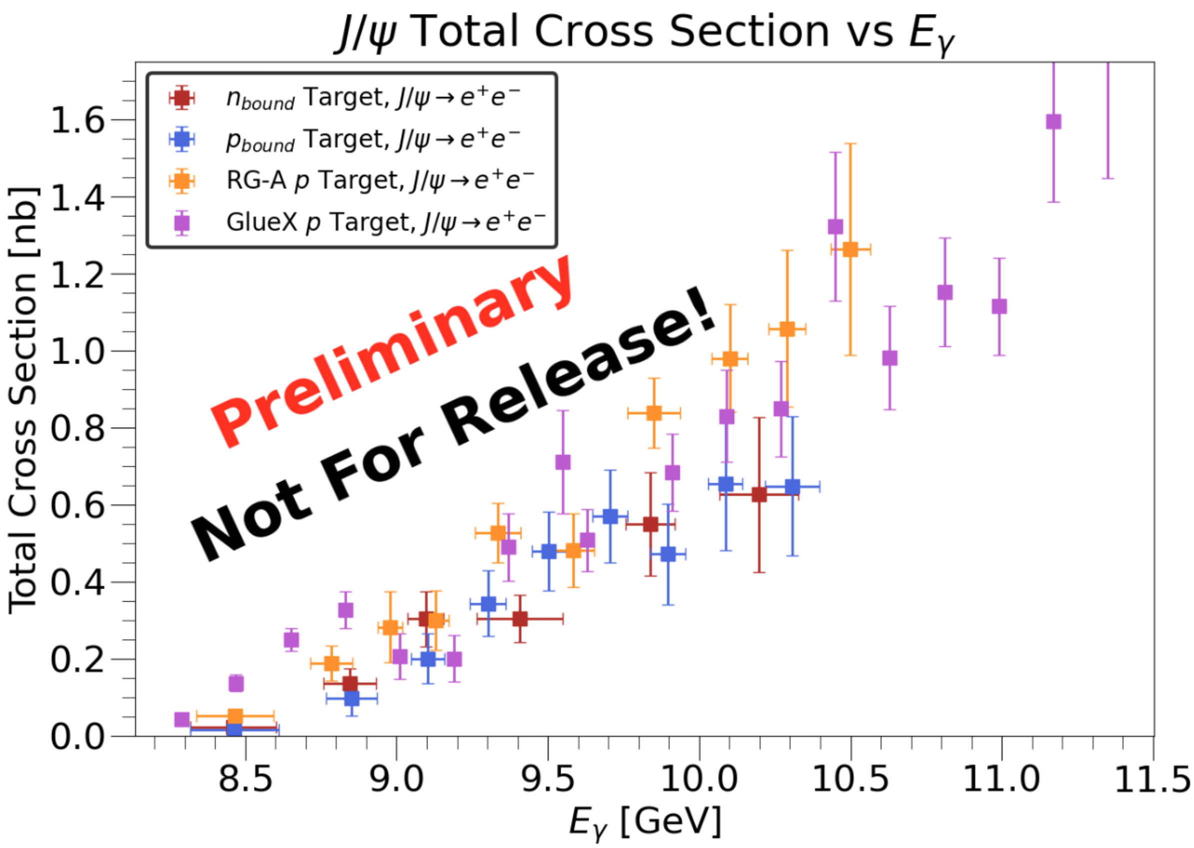

Figure 4: A comparison of the J/ψ photoproduction cross section produced on proton in GlueX and the RG-A experiment and on proton and neutron in the RG-B experiment. **This figure is not intended for release.**

6 Conclusion

The possibility to measure the gGFFs from J/ψ near-threshold photoproduction has sparked a great deal of interest in both experiment and theoretical interpretations of the data. Relating the J/ψ cross section to the gGFFs is dependent on the J/ψ production mechanism near threshold, and the current world data does not have the statistical accuracy to distinguish between different proposed production mechanisms. All previous estimates of the cross section have utilised a proton target. Comparing the cross section on proton and neutron will bring additional constraints to the J/ψ production mechanism. In the case of a dominant two-gluon production mechanism, a measurement of the cross section on the neutron would enable access to the neutron gGFFs. This release note shows the preliminary analysis towards a first measurement of J/ψ near-threshold photoproduction on the proton and the neutron in a deuteron target. The state of the analysis has been reviewed, and the preliminary cross section in arbitrary units shows good agreement between the cross sections produced on proton and neutron.

References

[1] T.-S. H. Lee, S. Sakinah, Yongseok Oh, Models of J/ψ photo-production reactions on the nucleon, *Eur. Phys. J. C* **58** 252 (2022).

[2] D. Kharzeev, Mass radius of the proton, *Phys. Rev. D* **104** 054015 (2021).

[3] H. Pagels, Energy-Momentum Structure Form Factors of Particles, *Phys. Rev.* **144** (1966).

[4] C. W. Misner, K.S. Thorne, J.A Wheeler, *Gravitation* W. H. Freeman 1973 Box 18.1.

[5] L. Frankfurt, M. Strikman, Two-gluon form factor of the nucleon and J/ψ photoproduction, *Phys. Rev. D.* **66**, 031502 (2002).

[6] D. Kharzeev, H. Satz, A. Syamtomov, and G. Zinovev, J/ψ Photoproduction and the Gluon Structure of the Nucleon, *Nucl.Phys. A* **661** 568 (1999).

[7] Y. Hatta and D.-L. Yang, Holographic J/ψ production near threshold and the proton mass problem, *Phys. Rev. D* **98** 074003 (2018).

[8] K.A. Mamo, I. Zahed, J/ψ near threshold in holographic QCD: A and D gravitational form factors, *Phys. Rev. D* **106** 086004 (2022).

[9] Y. Guo, X. Ji, Y. Liu, QCD analysis of near-threshold photon-proton production of heavy quarkonium, *Phys. Rev. D* **103**, 096010 (2021).

[10] Y . Guo, X. Ji, Y. Liu, J. Yang, Updated analysis of near-threshold heavy quarkonium production for probe of proton's gluonic gravitational form factors, *Phys. Rev. D* **108** 034003 (2023).

[11] Y. Guo, X. Ji, F. Yuan, Proton's gluon GPDs at large skewness and gravitational form factors from near threshold heavy quarkonium photoproduction, *Phys. Rev. D* **109** 014014 (2024).

[12] M.-L. Du, V. Baru, F.-K. Guo, C. Hanhart, U.-G. Meißner, A. Nefediev, I.Strakovsky, Deciphering the mechanism of near-threshold J/ψ photoproduction, *Eur. Phys. J. C* **80** 1053 (2020).

[13] D. Winney, *et al*, (Joint Physics Analysis Center), Dynamics in near-threshold J/ψ photoproduction, *Phys. Rev. D* **108** 054018 (2023).

[14] A. Ali *et al.* (GlueX Collaboration), First Measurement of Near-Threshold J/ψ Exclusive Photoproduction off the Proton, *Phys.Rev.Lett.* **123** 072001 (2019).

[15] S. Adhikari, *et al.* (GlueX Collaboration), Measurement of the J/ψ photoproduction cross section over the full near-threshold kinematic region, *ArXiv e-prints* arXiv:2304.03845v1 (2023).

[16] D. Duran, *et al.* (J/ψ -007 Collaboration), Determining the gluonic gravitational form factors of the proton, *Nature* **615** 813–816 (2023).

[17] M. Ungaro *et al.*, The CLAS12 Geant4 simulation, *Nucl. Instrum. Methods A* **959** 163422 (2020).

[18] D. Glazier, *elSpectro*, https://github.com/dglazier/elSpectro/tree/master.

[19] V.D. Burkert, *et al.*, The CLAS12 Spectrometer at Jefferson Laboratory, *Nucl. Inst. Methods A* **959** 163419 (2020).

[20] Y.G. Sharabian, *et al.*, The CLAS12 high threshold Cherenkov counter, *Nucl. Inst. Methods A* **968** 163824 (2020).

[21] M. Ungaro, *et al.*, The CLAS12 Low Threshold Cherenkov Counter, *Nuclear Inst. Methods A* **957** 163420 (2020).

[22] M.D. Mestayer, *et al.*, The CLAS12 drift chamber system, *Nucl. Inst. Methods A* **959** 163518 (2020)

[23] D.S. Carman, *et al.*, The CLAS12 Forward Time-of-Flight system, *Nuclear Inst. Methods A* **960** 163629 (2020).

[24] G. Asryan, *et al.*, The CLAS12 forward electromagnetic calorimeter, *Nucl. Inst. Methods A* **959** 163425 (2020).

[25] R. Tyson, J/ψ Near-Threshold Photoproduction off the Proton and Neutron with CLAS12, Ph.D. Thesis, University of Glasgow (2023).
Available online at https://theses.gla.ac.uk/83777/ .

[26] Y. Freund, R. E. Schapire, Experiments with a new boosting algorithm, *Proceedings of the 13th international conference on machine learning* 148–156 (1996).